# Dense Perovskite Membrane Reactors for Partial Oxidation of Methane to Syngas

**Chung-Yi Tsai, Anthony G. Dixon, William R. Moser, and Yi Hua Ma**
Center for Inorganic Membrane Studies, Dept. of Chemical Engineering, Worcester Polytechnic Institute, 100 Institute Road, Worcester, MA 01609

*The partial oxidation of methane to synthesis gas (syngas, $CO + H_2$) was performed in a mixed-conducting perovskite dense membrane reactor at 850°C, in which oxygen was separated from air and simultaneously fed into the methane stream. Steady-state oxygen permeation rates for $La_{1-x}A'_xFe_{0.8}Co_{0.2}O_{3-\delta}$ perovskite membranes in nonreacting air/helium experiments were in the order of $A'_x = Ba_{0.8} > Ba_{0.6} > Ca_{0.6} > Sr_{0.6}$. Deep oxidation products were obtained from a $La_{0.2}Ba_{0.8}Fe_{0.8}Co_{0.2}O_{3-\delta}$ disk-shaped membrane reactor without catalyst, with a 4.6% $CH_4$ inlet stream. These products were further reformed to syngas when a downstream catalytic bed was added. Packing the 5% $Ni/Al_2O_3$ catalyst directly on the membrane reaction-side surface resulted in a slow fivefold increase in $O_2$ permeation, and a fourfold increase in $CH_4$ conversion. XRD, EDS, and SEM analyses revealed structure and composition changes on the membrane surfaces. Oxygen continuously transported from the air side appeared to stabilize the membrane interior, and the reactor was operated for up to 850 h.*

## Introduction

Methane utilization has been drawing considerable attention recently due to the large amount of natural gas available to be upgraded, and the worldwide demand for low-cost transportation fuels. Technologies available for converting methane to liquid fuels are classified as either direct or indirect routes (Fox, 1993). Direct conversion of methane requires direct partial oxidation to methanol, formaldehyde, or others, or oxidative coupling to ethylene, to avoid the cost of the synthesis gas (syngas) preparation step in the direct route. The direct-conversion processes, however, have not yet been successful, because the desired products are more reactive than methane. Low product yield is normally encountered.

Syngas can be prepared either by steam reforming (Rostrup-Nielson, 1988), or by partial oxidation (oxyreforming) under oxygen-limited conditions. A typical steam-reforming reactor is operated at 15 to 30 atm and 850 to 900°C with a $Ni/Al_2O_3$ catalyst and a superficial contact time (based on the feed gases at STP) of 0.5 to 1.5 s. Unlike steam reforming [$CH_4 + H_2O \rightarrow CO + 3H_2$, $\Delta H(25°C) = +49.2$ kcal/mol], the partial-oxidation reaction [$CH_4 + 1/2O_2 \rightarrow 2H_2 + CO$, $\Delta H(25°C) = -8.5$ kcal/mol] produces stoichiometric syngas, at 13 atm within a shorter contact time and without further modification of the $H_2/CO$ ratio (2 to 1) for downstream processes, such as Fischer–Tropsch or methanol synthesis (Fox, 1993). Furthermore, an external energy supply is not needed for partial oxidation to syngas due to its exothermicity. The capital cost for the syngas synthesis step, therefore, may be reduced if conventional steam reforming can be completely or partially replaced by the partial-oxidation reaction.

Although very active catalysts for the partial oxidation of methane to syngas, with high CO and $H_2$ selectivities and high $CH_4$ conversion, have been reported (Ashcroft et al., 1990; Vermeiren et al., 1992; Hickman and Schmidt, 1993), large-scale plants have not yet been constructed. Since most of the catalysts discovered for exothermic syngas synthesis are active at high temperature ( > 700°C), a large adiabatic temperature rise at the front of the conventional co-fed reactor, which may cause reactor runaway, has to be carefully dealt with by reactor design. Reactor design, therefore, has centered on how to remove and use the heat of reaction efficiently. Some examples are the cyclic reactor (Blanks et al., 1990), in which flow direction was periodically reversed for heat exchange, and combined reforming, in which heat recovery from a second autothermal packed-bed reactor was provided for a primary steam reformer (Supp, 1989).

Correspondence concerning this article should be addressed to Y. H. Ma.

A second drawback of the partial-oxidation route from the economic point of view is that air is usually used to supply the oxidant. Since downstream processing requires the product stream to be free of nitrogen, either nitrogen must be separated from the syngas product mixture, or else oxygen must be separated from the air (usually cryogenically) before being fed to the syngas reactor. Although upstream nitrogen separation from air would be more favorable than costly downstream purification, a conventional cryogenic oxygen plant would be very costly in operation in conjunction with the partial-oxidation process. A novel reactor such as a membrane reactor, in which $O_2$ is separated from air and simultaneously fed into the methane stream without compromising the conversion and selectivity, would be an improved design.

Several advantages of using an oxygen-ion conducting membrane reactor, where methane and air feeds are separated, for the methane oxidation reaction include: (1) achieving high product selectivities; (2) employing air as an oxidant but eliminating $N_2$ contamination in the product; (3) circumventing flammability limits due to diffusion-limited operation; (4) reducing a large part of the cost of gas compression in downstream processing; and (5) avoiding the formation of environmental pollutants ($NO_x$) during high-temperature reactions.

Dense stabilized zirconias are well-known ionic-conductors in which oxygen ions transport through lattice vacancies due to the presence of the stabilizing materials and are neutralized by electrons from an external circuit. Alqahtany et al. (1993) studied the partial oxidation of $CH_4$ to syngas in a yttria-stabilized zirconia solid electrolyte cell. Although nearly 100% CO selectivity and 73% yield were achieved, the product formation rates were very low due to the low oxygen permeability of stabilized zirconia, despite the electrochemical pumping. The application of oxide membranes has so far been limited by their low $O_2$ permeation rates.

Two routes have been used to enhance the $O_2$ permeation rate. The first is to fabricate a very thin layer of oxygen-ion conducting material on top of a porous support (Hazbun, 1989; Xia et al., 1996; Ng et al., 1996). Although developments of techniques to make a very thin dense perovskite layer ( $< 20\ \mu$m) are in progress, the differences in the structure and thermal incompatibility between the oxide-layer material and the porous support need to be overcome, and with the reduction of diffusion resistance in the bulk oxide, oxygen permeation may become surface exchange-rate limited (Bouwmeester et al., 1992). In the second approach, new materials were developed with high oxygen permeability. With high electronic and ionic conductivities, mixed conductors such as some perovskites (generic formula $ABO_3$) have been reported to have permeation rates one or two orders of magnitude greater than those of stabilized zirconia (Teraoka et al., 1985).

The ideal perovskite structure is cubic with the generic formula $ABO_3$, where A is the larger cation in a twelvefold coordination, and B is the smaller cation in a sixfold coordination with oxygen ions. When the B ions can take a mixed-valence state, such as transition metals, the partial substitution of A site cations by other metal cations with lower valencies usually causes the formation of oxygen vacancies and a change in the valence state of the B ions in order to maintain the charge neutrality. The concentration of oxygen vacancies can also be increased by substituting ions of similar size but lower valence at the B site (Teraoka et al., 1988). The oxides, for example, $A_xA'_{1-x}B_yB'_{1-y}O_{3-\delta}$ (A = La; A' = Ba, Sr, Ca; B = Cr, Fe, Co, Mn; B' = Ni, Cu) may show both a high oxygen ion conductivity due to the high oxygen vacancy concentration, and a high electron conductivity due to the mixed-valence state (Mizusaki et al., 1985). Futhermore, at fixed temperature, the electronic conduction can be *n*-type or *p*-type, depending on the material properties and ambient oxygen partial pressure.

New reactor designs could feature the gradual supply of oxygen to the reactor through a dense perovskite layer that is a mixed conductor, thus allowing rapid oxygen permeation without the use of an external electrical circuit. In earlier work, we evaluated the possibilities of the use of such high oxygen-permeable membranes in catalytic membrane reactors by simulations of reactor performance via a mathematical model. A two-dimensional nonisothermal mathematical model was developed to simulate partial oxidation of methane to syngas in a tube-and-shell catalytic membrane reactor. The simulation results showed that the temperature rise in the exothermic partial oxidation reaction might be mitigated substantially by the use of a dense membrane reactor (Tsai et al., 1995a), which implied that a commercial-scale reactor could be possible. However, performance at the reactor scale was shown to be substantially limited by the oxygen permeabilities of the perovskite membranes used in the simulations (Tsai et al., 1995b).

The stability of perovskite membranes was addressed by Pei et al. (1995). Some perovskite materials have very high oxygen permeabilities but poor stabilities in a reducing atmosphere and at elevated temperature, for example, $SrCo_{0.8}Fe_{0.2}O_{3-\delta}$. The ideal material for constructing membrane reactors for the partial oxidation of methane to syngas, therefore, should have the following features: (1) high oxygen permeability; (2) good chemical stability under a harsh chemical environment; and (3) a stable lattice structure under changes in $O_2$ partial pressure. Our approach for material selection was partially based on literature studies (Tsai, 1996). Tejuca et al. (1989) pointed out that the most important prerequisite for a stable perovskite structure was the existence of a stable $BO_3$ skeletal sublattice. The stability of $LaBO_3$ in a hydrogen-reducing atmosphere at 1000°C was on the order of B = V ≈ Cr > Fe > Mn > Co > Ni (Nakamura et al., 1979). Unfortunately, perovskites with V or Cr at the B site usually have very low oxygen ionic conductivities. Furthermore, in a CO atmosphere, CO adsorption was favored for those B cations that have unfilled $e_g$ levels and an occupied $t2_g$ level, such as Mn and Co (Voorhoeve et al., 1977). As a compromise between the oxygen ionic conductivity and chemical stability, Fe appears to be the best choice for the B-site cation. Moreover, a mild cobalt substitution on the iron-rich B site also substantially increased the amount of oxygen desorption (Zhang et al., 1990). In the present work, different amounts and types of aliovalent cations ($Ca^{2+}$, $Sr^{2+}$, $Ba^{2+}$) were partially substituted for the $La^{3+}$ in a $LaFe_{0.8}Co_{0.2}O_{3-\delta}$ perovskite framework to attain the desired properties of high $O_2$ flux and stability under reducing conditions.

Balachandran et al. (1995) operated a tubular *nonperovskite* $SrCo_{0.5}FeO_x$ membrane reactor for the direct conversion of methane to syngas at about 900°C, in the presence of

an Rh-based reforming catalyst. $La_{0.6}Sr_{0.4}Co_{0.8}Fe_{0.2}O_x$ perovskite membranes were used as $O_2/N_2$ separators and methane coupling catalysts by ten Elshof et al. (1995). In the present work, we focused on the use of the mixed-conducting *perovskite* membrane due to its unique structure features for oxygen ionic and electronic conduction. Disk-shaped, $La_{0.2}Ba_{0.8}Fe_{0.8}Co_{0.2}O_{3-\delta}$ membrane reactors were selected to demonstrate (1) the concept of simultaneous reaction and oxygen separation from air; (2) the effect of reactor configurations on the membrane conversion, product selectivity, and oxygen permeation rate; and (3) the long-term stability under reaction conditions.

## Experimental Studies

### *Processing of perovskite disks*

The processing of perovskite disks includes powder preparation, shape-forming, and sintering processes. Powder preparation was modified from the citrate pyrolysis method (Blank et al., 1988). Stoichiometric amounts of corresponding ultra-high-purity metal nitrates were dissolved in nitric acid. Ultrapure metal nitrates (99.995 ~ 99.999%) were purchased from Aldrich except for $Ca(NO_3)_3 \cdot 4H_2O$ (Alfa/Johnson Matthey, 99.98%). Citric acid was then added to the solution with an acid-to-metal-mole ratio of 2 to 1. The total volume of the mixture was kept as small as possible by dissolving the mixture of metal nitrates into ultrapure nitric acid (70%). $NH_4OH$ (30%), loaded in a burette, was then gradually added to the stirred nitrate solution. A yellow precipitate was formed during the titration, but was later dissolved with the further addition of $NH_4OH$. The pH of the solution was adjusted to near 9. A complete homogeneous phase was then formed and agitated overnight.

The gel-type homogeneous phase was then poured into a 3-L beaker and evaporated on a hot plate (Corning) at around 200°C. Bubbles were formed vigorously and the solution became thicker. There was no evidence that selective precipitation was occurring. Spontaneous combustion was initiated by the ammonium nitrate ($NH_4NO_3$). The mouth of the 3-L beaker was covered with a fine sieve to prevent the loss of fine powders. Spontaneous combustion lasted around 10 s, and flame temperature was around 500°C in the beaker. Due to a limited amount of water in the nitrate solution in the present work, a large swollen viscous mass was not observed, in contrast to the study of Blank et al. (1988).

To achieve phase purity or reduce the residual carbon, particles were calcined for 5 h in air at 900°C with typical heating and cooling rates of 2°C/min. The soft particles were then crushed and ground in an agate mortar using an agate pestle. Membrane disks were obtained by pressing powders in a KBr die to 668 MPa. Green disks were sintered in air at 1,200°C for 10 h with heating and cooling rates of 2°C/min. The densities of the sintered membranes were close to theoretical values. After polishing on both surfaces, a sintered disk-shaped membrane of 0.55-mm thickness was mounted on a quartz tube using a gold ring seal (Tsai, 1996). For long-term permeation or reaction studies, solid-state gold sealing was superior to Pyrex-ring sealing, in which viscous glass could gradually interact with the membrane surface, causing disintegration of the membrane. The final area of the membrane disk, exposed to either air or diluted methane, was 0.283 $cm^2$ ($D$ = 0.6 cm).

### *Catalyst preparation*

Fine 5% $Rh/Al_2O_3$ powders, purchased from Aldrich, were pressed to 223 MPa in a KBr die to form solid pellets, without binder. Twenty ~ 40 mesh particles were then obtained by crushing the pellets. Five percent $Ni/\alpha\text{-}Al_2O_3$ was prepared by impregnating the support, amorphous aluminum oxide (Baker), with an aqueous solution of $Ni(NO_3)_2 \cdot 6H_2O$ (Aldrich) to yield a nominal metal loading of 5 wt. %. The particles were dried at 60°C for 24 h, and then calcined in air at 600°C for 4 h. Particles with sizes of 120 to 180 $\mu$m were further compressed to 148 MPa without binder to form pellets, which were then calcined at 1,000°C for 5 h. Twenty- to 40-mesh catalyst particles were again obtained by crushing the pellets. The color of the particles turned from green to dark blue after calcination.

### *Membrane reactor configurations and operation*

Gases of commercial purity, $CH_4$ (99.97% min, Matheson ultra-high-purity) and air (Airco) were used without further purification. Helium (Airco, < 99.9950%) flowed through an adsorptive oxygen trap (Oxy-Purge N, Alltech) to remove oxygen and moisture before being introduced to the system. The experimental layout is shown in Figure 1. Mass-flow controllers (Brooks 5850C), which were calibrated by a digital bubble flowmeter (Alltech) regulated the flow of gases into the reactor. An electronic pressure transducer (MKS Instruments Inc.) was used to accurately detect the reactor pressure, and a back-pressure regulator (Tescom Co.) was used to maintain the permeate-side pressure to 780 mmHg. A programmable temperature controller (Eurotherm 818 programmer) controlled a precalibrated vertical three-section furnace

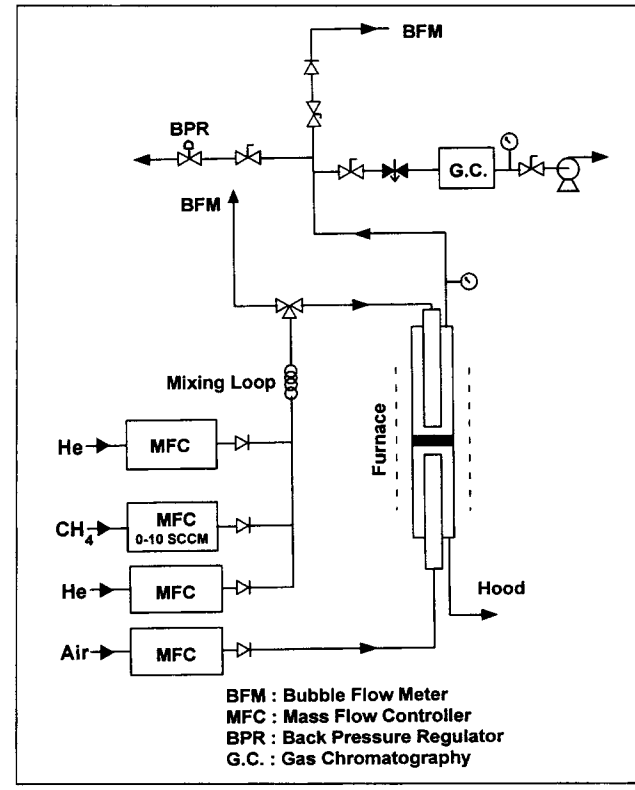


**Figure 1. Experimental apparatus.**

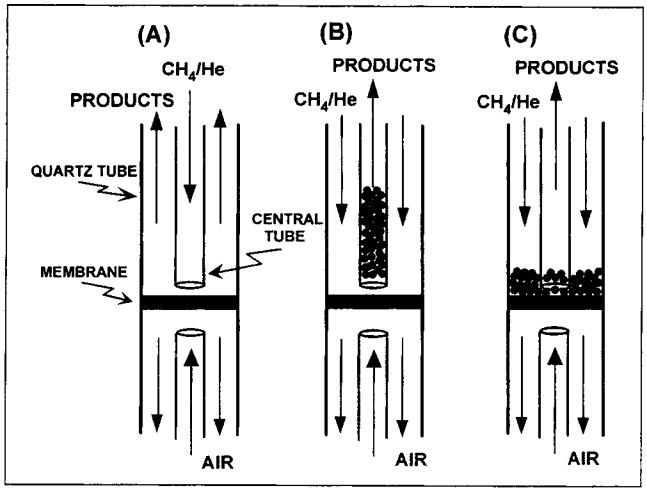


**Figure 2. Three configurations of disk-shaped membrane reactors.**

with K-type thermocouples (Omega), allowing the reaction zone to be operated either isothermally or in a temperature programmed mode.

Three reactor configurations were used and are illustrated in Figure 2. The diameters of the quartz reactor tube were 6 mm ID and 12 mm OD. The clearance between the end of the central tube (2 mm ID and 4 mm OD) in the reactor and the membrane surface was less than 3 mm for all three cases. It was important to keep the clearance as small as possible to reduce the dead volume. One side of the membrane was exposed to air [200 $cm^3$ (STP)/min], while the other side was exposed to either diluted methane in the reaction runs, or to helium in the permeation runs. Inlet dilution was needed to prevent a possible explosion caused by the instant mixing of $O_2$ and methane, in the event of membrane breakage. In the reaction runs, 4.6% diluted methane, in general, was used for the feedstock, unless otherwise specified. Reactors B and C were loaded with 85 mg of unreduced catalyst particles (5% $Rh/Al_2O_3$ or 5% $Ni/Al_2O_3$). The temperature around the membrane was controlled at 850°C for all cases. The length of the catalytic bed for reactor B was 5.5 cm, in which both ends of the tube were plugged with quartz wool. The inlet of the catalyst bed was about 8 mm away from the surface of the membrane. For reactor C, catalyst particles were packed directly on the top of the membrane. The bed height was 4.5 mm; therefore, the central tube protruded into the catalyst bed.

During the changeover between each reactor configuration, the membrane was inevitably exposed to the atmosphere. However, the membrane was continuously maintained at 850°C without being disturbed. Before the catalyst particles were introduced into the reactor, the previous procedure for the oxygen permeation measurement was applied, at 850°C. For the reactor B configuration, the catalyst was packed into a 2-mm-ID quartz tube and then lowered down to the heating zone, while for the reactor C configuration, the catalyst was dropped onto the membrane surface. To start each reactor experiment, the reactor was first purged with helium until the air was completely replaced, and then 4.6% $CH_4$ was introduced into the system. During each reactor experiment, the reactors were run continuously 24 h a day, following the sequence from reactor A to C.

The inlet methane concentration and the product gases were analyzed by on-line gas chromatography. The on-line gas chromatograph (HP5890 Series II) was equipped with two automatic valves, a sampling valve and a bypass valve, and HP Chemstation computer software for data collection and analysis. A serial/bypass configuration was arranged for two isothermal columns (80°C), Hayesep Q and molecular sieve 13X. The injection of sample gases directed the mixture of $H_2$, $O_2$, $N_2$, $CH_4$, CO, $CO_2$, and $C_2$'s ($C_2H_4$ and $C_2H_6$) through the Hayesep Q column. $H_2$, $O_2$, $N_2$, $CH_4$, and CO were eluted earlier than $CO_2$ and the $C_2$'s from the Hayesep Q column, and then quickly entered the serial-arranged molecular sieve 13X column. Once the $H_2$, $O_2$, and $N_2$ were eluted from the molecular sieve 13X column and passed to the thermal conductivity detector, a bypass valve was activated to deadend the molecular sieve 13X column and direct the outlet of the Hayesep Q column to the detector. Once $CO_2$, $C_2H_4$, and $C_2H_6$ had eluted from the Hayesep Q, the valve was again activated, and $CH_4$ and CO were eluted from the molecular sieve column to the detector. An external standardization was used for product analysis. Multiple-point calibration curves were created, and recalibrated routinely for long-term studies. The quantity of $H_2O$ was calculated by a hydrogen atomic balance. The oxygen permeation rate was calculated from the measured inlet flow rate and the molar fractions of O-containing product gases, such as CO, $CO_2$, $O_2$, and $H_2O$. The carbon balance during all of the experiments was closed to within 5%. The separation of $O_2$ and $N_2$ was crucial for leak checking on the membrane and the gold seal. The leak-oxygen could be calculated from the leak-nitrogen. In the reaction experimental results, the leak-oxygen flux, which accounted for 0 to 2% of the total oxygen flux, was subtracted from the total oxygen flux.

### *Characterization of membrane materials*

EDS-scanning electron microscopy (JEOL 840) equipped with a Kevex Quantum detector was used to characterize the perovskite powders and membrane disks. The X-ray patterns, for either powders or membranes, were taken by using General Electric diffractometer model XRD-5 with a graphite monochromator, using CuK$\alpha$ radiation (50 kV/15 mA). The surface-area measurements of the various powder samples were carried out using the multipoint BET method by Autosorb-1 automated gas sorption system (Quantachrome Co.). Nitrogen gas at 77 K was used as the adsorbate. Quasi-elastic light-scattering spectroscopy (QELSS) is based on fluctuations in the intensity of scattered light caused by the Brownian motion of particles, and was applied to the observation of particles ranging from 5 nm to 5 $\mu$m in a gradient-free equilibrium solution (Phillies, 1990). The powder melting point was observed by DTA (Harrop Industries Inc.).

## Results and Discussion

### *$O_2$ permeation rates in perovskite membranes*

The oxygen permeation rate measurements were operated at a helium flow rate of 52.5 $cm^3$(STP)/min and an air flow rate of 200 $cm^3$(STP)/min, for all membranes. A typical re-

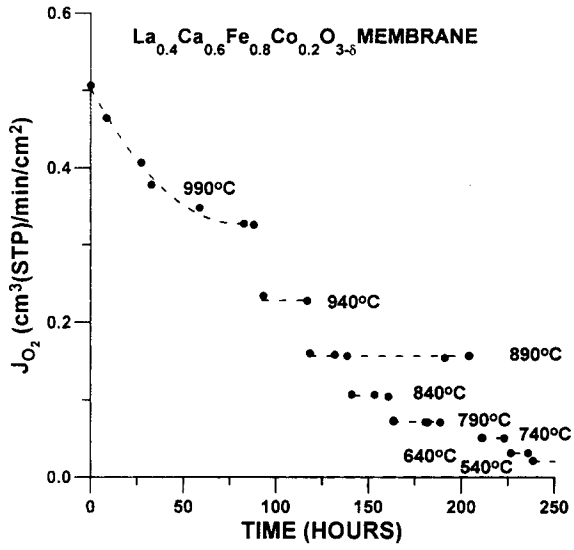


**Figure 3. Time course of oxygen permeation rates for $La_{0.4}Ca_{0.6}Fe_{0.8}Co_{0.2}O_{3-\delta}$ membrane at varied temperature.**

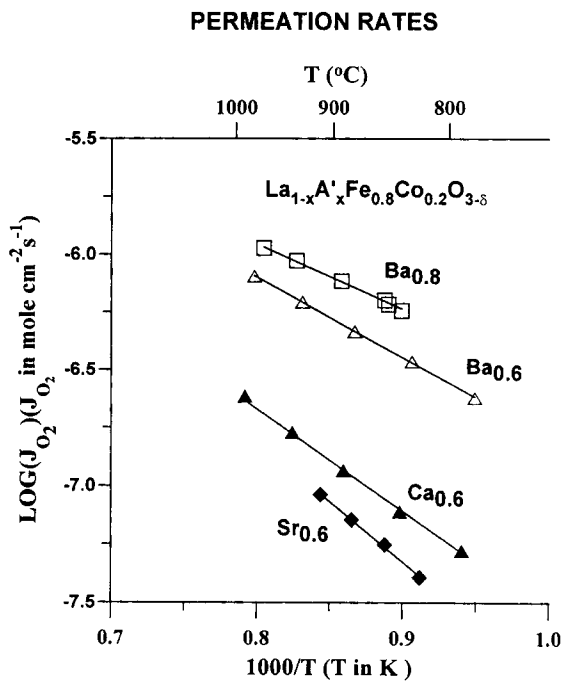


**Figure 4. Arrhenius plots of steady-state oxygen permeation rates in a helium/air gradient for perovskites.**

sult for one material, $La_{0.4}Ca_{0.6}Fe_{0.8}Co_{0.2}O_{3-\delta}$, is shown in Figure 3. Oxygen permeation rates for this membrane declined gradually with time on stream at 990°C, which might have been due to the lessening of initial surface oxygen desorption rates and the readjusting of the lattice structure from the as-synthesized state. The $O_2$ permeation rate decreased from the initial value of 0.5 $cm^3/min/cm^2$ to the steady-state value of 0.3 $cm^3/min/cm^2$ in 100 h. The gradual decrease in the initial $O_2$ permeation rate was similar to what had been observed previously in $La_{0.2}Sr_{0.8}Co_{0.8}Fe_{0.2}O_{3-\delta}$ membrane (Tsai et al., 1995b). Once a steady state was reached, the temperature was cooled down at a rate of 1°C/min to another temperature level for the next steady-state condition. The second steady state was reached much more quickly than the first steady state. The steady-state $O_2$ permeation rate was a function of temperature, and was unaffected by the thermal history as shown by the $O_2$-permeation data at 890°C (Figure 3). Generally speaking, membranes with high initial oxygen permeation rates spent less time in reaching steady state than those with low initial oxygen permeation rates. Kruidhof et al. (1993) observed a more dramatic decline in the $O_2$ permeation rate, one order of magnitude in 100 h, for the $La_{0.6}Sr_{0.4}CoO_{3-\delta}$ membrane at 750°C. They attributed their observation to the gradual development of an ordered structure, which could have been unfavorable to oxygen transport.

A theoretical mechanism for $O_2$ permeation through a perovskite membrane was developed by Tsai (1996), in which, based on a simple point-defect model, the surface reactions were coupled with the bulk reaction in order to interpret the oxygen ionic transport through either *p*- or *n*-type perovskites. A summary of $O_2$ permeation rates for the perovskites in the present study is shown in Figure 4. These materials exhibited very high electronic *p*-type conductivity under our operating conditions, so that oxygen permeation was limited either by diffusion of oxygen vacancies in the bulk oxide or by the surface dissociation rate. The latter phenomenon was assumed negligible in the theoretical formulation for the calculation of the activation energy. For a thin membrane of thickness, $L$, the preexponential factor, $A$, and the activation energy, $E_a$, were acquired by correlating the experimental data in Figure 4 with the equation

$$J_{O_2} = Ae^{-E_a/RT}\frac{T}{L}\ln\left(\frac{P^{I}_{O_2}}{P^{II}_{O_2}}\right). \quad (1)$$

The oxygen partial pressure on the permeation side, superscript II, is lower than that on the air feed side, superscript I, and $R$ is the gas constant. An important trend was found for the membranes shown in Table 1, that the higher the $O_2$ permeation rate (or oxygen ionic conductivity), the lower the activation energy. The interpretation of this observation, associated with the average metal–oxygen bond energy and the free lattice volume, is addressed elsewhere (Tsai et al., 1996). Steady-state oxygen permeation rates for the family of $La_{1-x}A'_xFe_{0.8}Co_{0.2}O_{3-\delta}$ perovskites were on the order of $A'_x = Ba_{0.8} > Ba_{0.6} > Ca_{0.6} > Sr_{0.6}$. Oxygen permeation rates could therefore be increased by one order of magnitude by engineering the A-site cation substitution. The highest permeation rate among those materials studied had a permeability one order of magnitude higher than those typical of stabi-

**Table 1. Oxygen Ionic Transport Properties of Perovskite Membranes**

| Compositions $La_{1-x}A'_xFe_{0.8}Co_{0.2}O_{3-\delta}$ $A'_x$ | Activation Energy $E_a$ (kJ/mol) | Preexponential Factor, $A$ (mol/cm·s-K) |
|---|---|---|
| $Ba_{0.8}$ | 62.7±1.5 | $7.34\times10^{-9}$ |
| $Ba_{0.6}$ | 72.4±0.7 | $1.03\times10^{-8}$ |
| $Ca_{0.6}$ | 95.3±0.9 | $1.93\times10^{-8}$ |
| $Sr_{0.6}$ | 105.6±3.8 | $3.41\times10^{-8}$ |

lized zirconias. The $La_{0.2}Ba_{0.8}Fe_{0.8}Co_{0.2}O_{3-\delta}$ membrane, with the highest oxygen permeation rate, was adopted for the reactor experiments.

To observe high-temperature phases, the membrane samples, annealed in a controlled atmosphere for 48 h, were quenched into liquid nitrogen. In Figure 5, the XRD patterns for the $La_{0.2}Ba_{0.8}Fe_{0.8}Co_{0.2}O_{3-\delta}$ membrane show that the lattice parameters were expanded isotropically both in helium and in air at elevated temperature. The lattice expansion was due to the loss of lattice oxygen at elevated temperature, and might be explained by charge compensation. Some of the $Fe^{4+}$ and $Co^{4+}$ ions may have been reduced to $Fe^{3+}$ and $Co^{3+}$ ions due to the loss of lattice oxygen, and the ionic radii of $Fe^{3+}$ and $Co^{3+}$ ions are larger than those of $Co^{4+}$ and $Fe^{4+}$ ions, respectively. Furthermore, it is important that the cubic structure be observed throughout a large temperature range both in air and in a helium atmosphere. Materials that expand evenly on heating are frequently much more stable during thermal cycling. The $La_{0.2}Ba_{0.8}Fe_{0.8}Co_{0.2}O_{3-\delta}$ membrane had a stable structure at high temperatures and under a reducing atmosphere, due to high iron content in the B-site. Moreover, the perovskite (110) peak in the XRD pattern was shifted far more to the low-angle side, due to lattice expansion, for the sample in helium than for that in air at 850°C. Calculated results suggested that the lattice expanded 0.62% due to shifting the ambient atmosphere from air to helium.

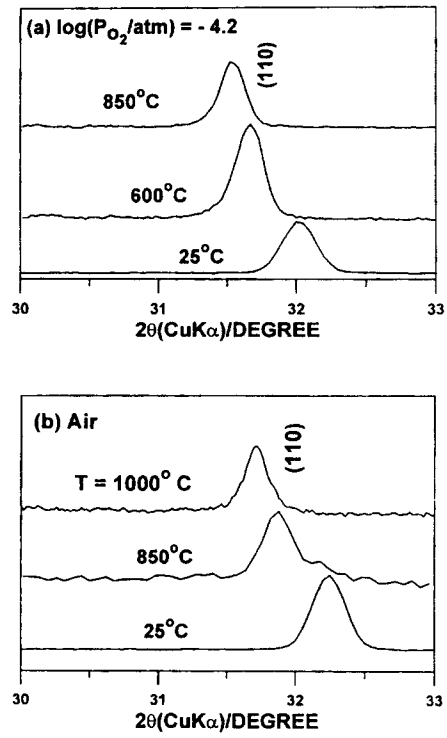


**Figure 5. X-ray diffraction patterns for the as-quenched $La_{0.2}Ba_{0.8}Fe_{0.8}Co_{0.2}O_{3-\delta}$ (LB8FC) membrane either in helium (a) or in air (b) at elevated temperature.**

### *Effects of reactor configurations on oxygen permeation rates and product profiles*

The long-term stability of the membrane reactors was investigated using reactor configurations (Figure 2) that were consecutive modifications of the $La_{0.2}Ba_{0.8}Fe_{0.8}Co_{0.2}O_{3-\delta}$ membrane reactor. The same perovskite membrane was used throughout all the reactor configuration experiments. Methane conversion, CO selectivity, and $C_2$ selectivity (on a carbon atom basis) were defined as follows:

$$CH_4 \text{ conversion} = \frac{F_{CH_4,\text{inlet}} - F_{CH_4,\text{outlet}}}{F_{CH_4,\text{inlet}}} \quad (2)$$

$$C_2 \text{ selectivity} = \frac{2(F_{C_2H_4} + F_{C_2H_6})}{F_{CO} + F_{CO_2} + 2(F_{C_2H_4} + F_{C_2H_6})} \quad (3)$$

$$CO \text{ selectivity} = \frac{F_{CO}}{F_{CO} + F_{CO_2} + 2(F_{C_2H_4} + F_{C_2H_6})}. \quad (4)$$

A summary of the physical properties of the $La_{0.2}Ba_{0.8}Fe_{0.8}Co_{0.2}O_{3-\delta}$ membrane selected for the reaction experiments is given in Table 2.

The first set of reactor experiments used configuration A with no catalyst. With a flow rate of 34.2 cm$^3$(STP)/min, the product stream in blank reactor A at 850°C contained the unreacted $CH_4$, permeated $O_2$ ( ~ 0.54%), $CO_2$, CO, and $C_2$'s (mainly $C_2H_6$) (Figure 6). The $O_2$ utilization accounted for only 13% of the permeated oxygen. The conversion of $CH_4$ was about 5%, which may have been due to either the gas-phase reaction, or the catalytic reaction on a small active area of the membrane surface. The deep methane oxidation reaction dominated; therefore, the main product was $CO_2$. The $CH_4$ conversion, the $O_2$ permeation rate, and the concentration ratio of $CH_4$ to $O_2$ were stable for 250 h; however, the $CO_2$ selectivity slightly decreased and eventually leveled off, which was accompanied by a slight increase in $C_2$ selectivity. The gradual increase in $C_2$ selectivity may have been due to the partial decomposition of the stoichiometric perovskite on the membrane surface into the more active BaO phase (Dissanayake et al., 1993).

In the second set of reactor experiments, 85 mg of 5% $Rh/Al_2O_3$ catalyst was loaded in reactor B (Figure 2b). Before entering the downstream catalyst bed, the 4.6% diluted methane inlet stream, with a flow rate of 55.2 cm$^3$(STP)/min, resulted in a 3% $CH_4$ conversion at 850°C (Figure 7), and a similar product composition to that in reactor A. The down-

**Table 2. Physical Properties of the $La_{0.2}Ba_{0.8}Fe_{0.8}Co_{0.2}O_{3-\delta}$ Membrane**

| | |
|---|---|
| *Powders* | |
| Formula | $La_{0.2}Ba_{0.8}Fe_{0.8}Co_{0.2}O_{3-\delta}$ |
| Surface area (m$^2$/g) | 7.734 (uncalcined)<br>2.601 (900°C, calcined) |
| Particle size (nm) | 20 |
| Melting point (°C) | 1350 ~ 1410 |
| *Membrane* | |
| Crystal structure | Cubic |
| Thickness (cm) | 0.055 |
| Density (g/cm$^3$) | 6.2 |
| % Theoretical density | 98% |
| Surface after sealing (cm$^2$) | 0.283 |

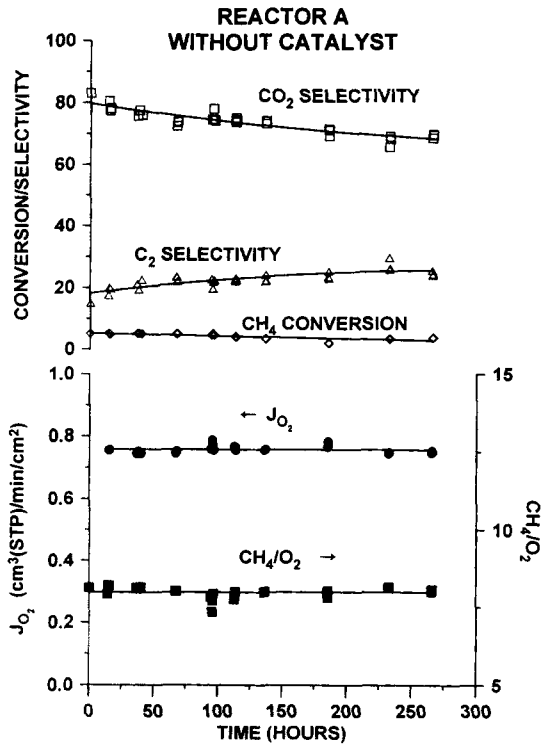


**Figure 6. Blank run for the membrane reactor (reactor A).**

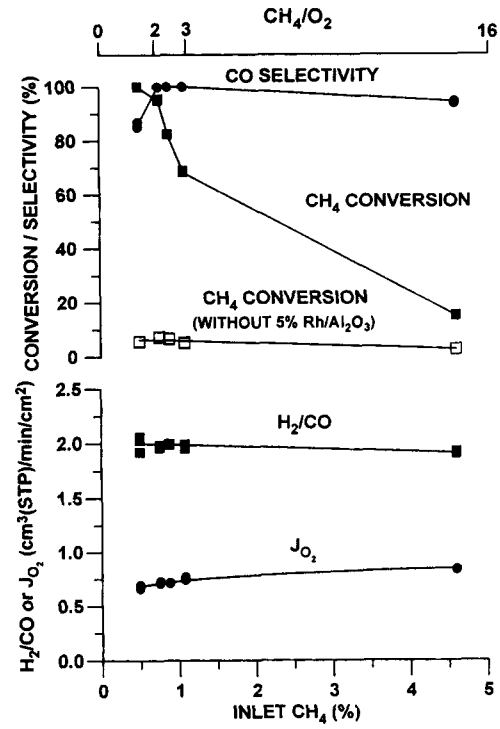


**Figure 7. Effect of methane dilution in reactor B, with catalyst 5% $Rh/Al_2O_3$.**

Upper $x$-axis, $CH_4/O_2$, designates the ratio of methane to permeated molecular oxygen at the inlet of catalytic bed.

stream catalyst bed did not affect oxygen permeability for the membrane, but did convert some of the remaining $CH_4$, permeated $O_2$, $CO_2$, CO, $H_2O$, and $C_2$'s further to CO and $H_2$. Oxygen concentration at the outlet of the catalyst bed was below detectable levels ( $< 10^{-5}$ atm) by gas chromatography. The effect of methane dilution is also shown in Figure 7. A decrease in methane inlet concentration dramatically increased $CH_4$ conversion, with a minor effect on both the $H_2/CO$ ratio and the oxygen permeation rate. When nearly 0.7% inlet methane concentration was employed, the CO selectivity reached almost 100%, with a $CH_4$ conversion of 95%. This dilution rate corresponded to a $CH_4/O_2$ ratio of close to 2, which is the stoichiometric reactant ratio for syngas synthesis ($CH_4 + 1/2O_2 \rightarrow 2H_2 + CO$). Further dilution and lowering of the $CH_4/O_2$ ratio was accompanied by a strong decline in CO selectivity.

Comparison was made between the two catalysts, 85 mg of 5% $Ni/Al_2O_3$ or 5% $Rh/Al_2O_3$, in reactor B under identical operating conditions (Figures 8 and 9). Although the steady-state $CH_4$ conversion was about 15% for both catalysts at 850°C, the initial $CH_4$ conversion and CO selectivity for the 5% $Rh/Al_2O_3$ catalyst were higher than those for 5% $Ni/Al_2O_3$. The CO selectivity for the 5% $Rh/Al_2O_3$ catalyst decreased and eventually reached 95%, while the CO selectivity for the 5% $Ni/Al_2O_3$ catalyst remained at 99%. Moreover, the concentration ratio of $H_2/CO$ indicated that the 5% $Ni/Al_2O_3$ catalyst was more selective to $H_2$, while the 5% $Rh/Al_2O_3$ catalyst was more selective to CO. Compared to reactor A, reactor B showed no increased oxygen permeation rates, even though the diluted methane inlet flow rate was higher in reactor B [55.2 $cm^3$(STP)/min]; therefore, the higher $CH_4$ conversion in reactor B was mainly due to the utilization of the permeated molecular oxygen by the downstream catalyst bed. The dominant product in reactor B was CO, in contrast to $CO_2$ in reactor A, which implied that the overall reaction included the $CO_2$ and $H_2O$ reforming reactions in reactor B.

The long-term stability of the oxygen permeation rates is summarized in Figure 10, following the order of the described reaction experiments. Oxygen permeation rates were

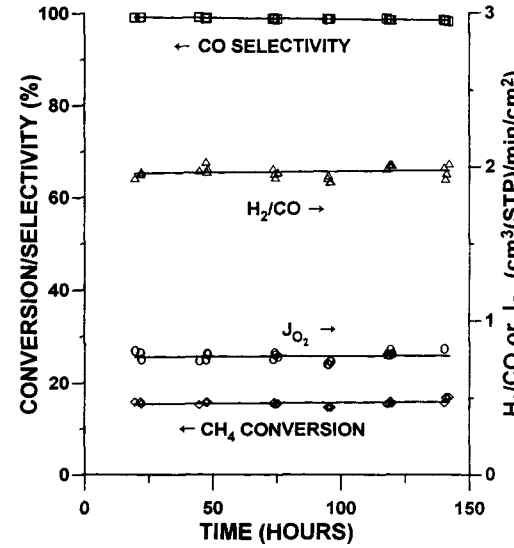


**Figure 8. Long-term stability of reactor B loaded with catalyst 5% $Ni/Al_2O_3$.**

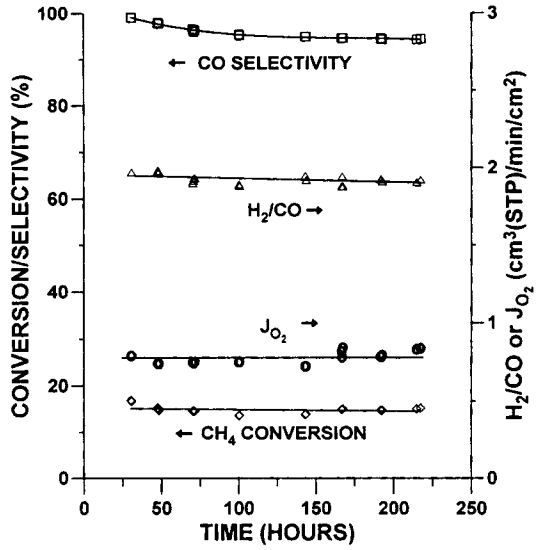


**Figure 9. Long-term stability of reactor B loaded with catalyst 5% $Rh/Al_2O_3$.**

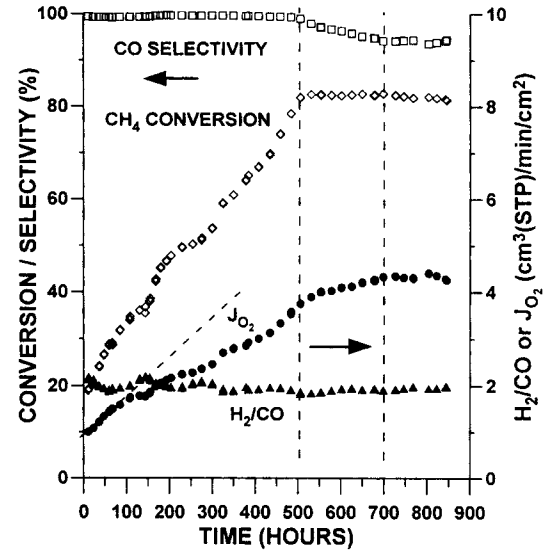


**Figure 11. Long-term stability for the reactor C with 5% $Ni/Al_2O_3$ catalysts on top of the membrane surface.**

measured during the intermissions between reaction experiments. For comparison, the permeation experiments were operated at a constant flow rate and direction, in which pure helium [50.2 $cm^3$(STP)/min] flowed from the central tube toward the membrane surface without any catalyst packing. Although a single membrane was used for all of the experiments, the oxygen permeation rates were stable at the start of every reaction experiment, over a period of 60 days.

In the third set of reactor experiments, configuration C had the catalyst, 85 mg of 5% $Ni/Al_2O_3$, packed on the top of the membrane, at 850°C (Figure 2c). The central tube protruded into the catalyst bed. The diluted methane with flow rate 55.2 $cm^3$(STP)/min passed through the catalyst bed to reach the central tube outlet. The oxygen concentration in the effluent was below detectable levels. The reaction was run continuously for over 850 h (Figure 11). From 0 to 500 h, the $CH_4$ conversion increased substantially from 17% to 80%, along with an increase in $O_2$ permeation rate. The $CH_4/O_2$ mixing ratio in the catalyst bed decreased from 12.2 to 2.5 due to the increase in the $O_2$ permeation rate. CO selectivity and $H_2/CO$ ratio were essentially unchanged through 500 h. From 500 h to 700 h, conversion leveled off while CO selectivity decreased, and the $O_2$ permeation rate continued to increase, but more slowly. The slow increase in $O_2$ permeation rate did not contribute to an increase in $CH_4$ conversion but to a decrease in CO selectivity due to the formation of $CO_2$. The decrease in the CO selectivity might be attributed to the lower $CH_4/O_2$ mixing ratio, caused by the higher $O_2$ permeation rate, similar to the observation in Figure 7 of decreased CO selectivity for ratios close to the stoichiometric reactant ratio of 2. For times greater than 700 h, the oxygen permeation rate leveled off together with the $CH_4$ conversion and CO selectivity.

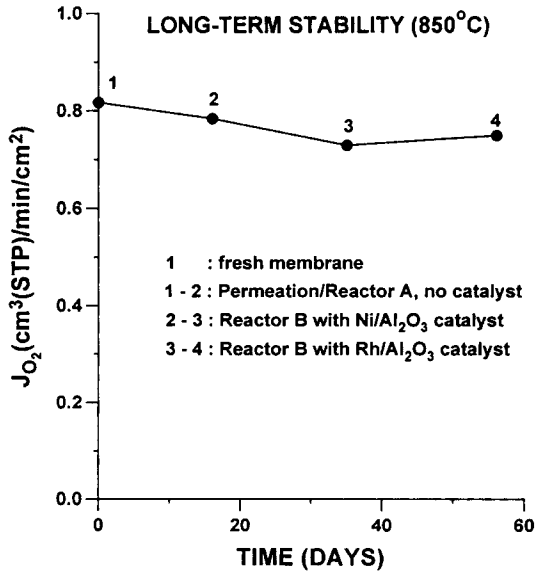


**Figure 10. Long-term stability for the $La_{0.2}Ba_{0.8}Fe_{0.8}Co_{0.2}O_{3-\delta}$ (LB8FC) membrane.**

Reactors B and C were operated under oxygen-limited conditions. $CH_4$ conversion depended on the amount of oxygen transported through the membrane. The downstream catalyst bed in the reactor B configuration for the syngas reaction did not increase the oxygen permeation rates over those in the reactor A configuration with no catalyst. When a bed of catalyst was packed on the top of the membrane surface, in the reactor C configuration, the oxygen permeation rates gradually increased to five times their initial configuration B value. Under reaction conditions, the permeability for this material was up to 1.5 orders of magnitude higher than that of stabilized zirconias.

XRD, EDS, and SEM analyses revealed the surface structure or composition changes of the perovskite, $La_{0.2}Ba_{0.8}Fe_{0.8}Co_{0.2}O_{3-\delta}$, membrane after long-term reactor operation. XRD patterns showed that doublet peaks were found in every characteristic peak for the cubic-phase perovskite on the reaction-side surface, while some shoulders were found in the characteristic peaks on the air-side surface. This would indicate that two perovskite phases with close lattice parame-

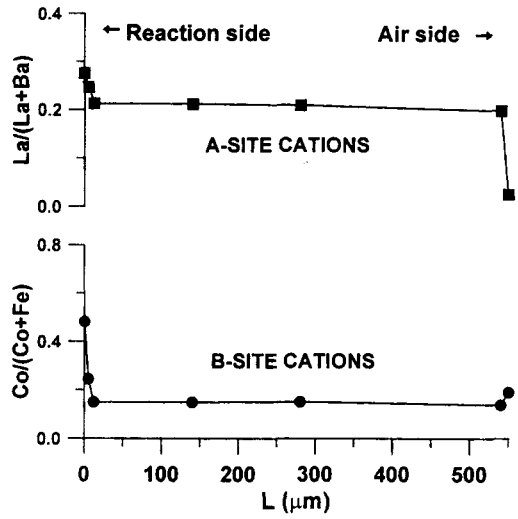


**Figure 12. Crosswise EDS composition analyses.**

Atomic ratio vs. the depth of membrane from the reducing-side surface ($L = 0$ $\mu$m) to the air-side surface ($L = 550$ $\mu$m).

ters might have coexisted on the reaction side. Furthermore, a strong BaO peak was observed on the air-side surface compared to that on the reducing-side surface. Although the segregation mechanism was not clear, it might be mainly attributed to the charge compensation mechanism due to oxygen anion dissociation on the air-side surface and migration from the air side to the reducing side. EDS analyses for the membrane cross-sectional area showed that the composition changes were preferentially located near both surfaces (Figure 12). Barium content was significantly increased on the air-side surface while a slightly higher cobalt content was found on the reducing-side surface. The composition in the middle of the membrane cross-sectional area was similar to that of the fresh membrane. SEM micrographs of membrane cross-sectional area showed a two-layer structure near the reaction-side surface. A fine-particle layer observed on the reaction side surface was around 2 $\mu$m thick. Under the fine-particle layer, big grains were broken down to 0.2 $\mu$m fine grains. This layer extended to a depth of around 10 $\mu$m. In contrast to near the reaction-side surface, a SEM micrograph near the air side showed a solid crystallized surface. Apparently, the surface near the reaction side was affected by the reducing atmosphere while the rest of the membrane was stabilized by the oxygen transport from the air side. Further details of the membrane characterization are presented elsewhere (Tsai et al., 1996).

### *Oxygen transport scheme for reactor configuration C*

Based on the evidence from XRD, SEM, and EDS, the gradual oxygen-permeation-rate increase in reactor configuration C was interpreted as follows. When the catalyst was packed on the top of the membrane surface, the gas-phase oxygen was consumed completely by the partial oxidation reaction. A reducing atmosphere developed in the catalyst bed, which influenced the membrane surface. Lattice oxygen started being removed; therefore, a fast increase in the oxygen permeation rate within the first 50 h was observed (Figure 11). The membrane surface material was transformed into a structure that was more favorable to oxygen transport. The surface oxygen exchange rate also increased, causing the increase in permeation rates.

Oxygen from the air side could not compensate for the loss of lattice oxygen on the reaction-side surface due to the relatively low oxygen transport rate across the membrane. The increase in oxygen permeation rates slowed down from 50 h to 700 h. The bulk membrane structure gradually adjusted to accommodate the oxygen partial pressure gradient across the membrane until the structure was fully developed. Some $BaCO_3$ was formed by the surface decomposition associated with the gaseous species. Barium segregation on the air-side surface was due to the long-term oxygen-ion migration accompanied by barium-ion migration in the opposite direction at high temperature. The surface segregation and decomposition might have eventually contributed to the slower increase in the oxygen permeation rate. The significant amount of $CO_2$ produced after 500 h was attributed to the reaction kinetics, similar to the packed-bed studies of Dissanayake et al. (1991), in which a lower $CH_4/O_2$ inlet mixing ratio in the catalyst bed was more favorable to $CO_2$ production. A less reducing atmosphere was gradually developed near the membrane surface due to the increase in $CO_2$ concentration. This slowed and eventually stopped the solid-state transformation of the membrane material. The increase in the oxygen permeation rate further slowed down, and the permeation rate eventually reached steady state.

## Conclusions

A range of perovskite materials was synthesized $(La, A')(Fe, Co)O_{3-\delta}$ to attain the desired properties of high $O_2$ flux and stability under reducing conditions. The atomic ratio of Fe to Co on the B-site of the perovskites was designated to be four, which gave a stable perovskite framework and allowed higher low-valent cation substitution on the A-site of the perovskites to attain the desired property of high $O_2$ flux. Steady-state oxygen permeation rates for the family of $La_{1-x}A'_xFe_{0.8}Co_{0.2}O_{3-\delta}$ perovskite membranes in nonreacting air/helium experiments were in the order $A'_x = Ba_{0.8} > Ba_{0.6} > Ca_{0.6} > Sr_{0.6}$. Oxygen permeation rates could be increased by one order of magnitude by engineering the A-site cation substitution.

For the $La_{1-x}A'_xFe_{0.8}Co_{0.2}O_{3-\delta}$ membranes, the gradual decrease in the initial $O_2$ permeation rate in nonreacting air/helium experiments was attributed to the lessening of initial surface oxygen desorption rates and the readjusting of the lattice structure. Once the first steady-state $O_2$ permeation rate was reached, the following steady-state $O_2$ permeation rates were reached quickly, and were only a function of temperature. For the $La_{0.2}Ba_{0.8}Fe_{0.8}Co_{0.2}O_{3-\delta}$ membrane, the cubic structure was stable in air and in helium ($P_{O_2} \sim 10^{-4.2}$ atm) streams at elevated temperature, although the lattice expanded due to the loss of oxygen from the perovskite structure.

An $La_{0.2}Ba_{0.8}Fe_{0.8}Co_{0.2}O_{3-\delta}$ disk-shaped membrane reactor was tested for the partial oxidation of methane to syngas at 850°C. Three configurations of membrane reactors were employed to demonstrate the concept of simultaneous reaction and separation of $O_2$ from air, as well as the effect of

the reactor configuration on the $CH_4$ conversion, product selectivity, and $O_2$ permeation rate, for a long period. Without the addition of catatyst, $CO_2$, $H_2O$, $CH_4$, and $O_2$ were the main components in the product stream for the first, blank reactor. Further reforming in a downstream catalytic bed could convert $CO_2$, $H_2O$, $CH_4$, and $O_2$ into CO and $H_2$ in the second reactor configuration studied. A gradual increase of $O_2$ permeation rate to five times the initial value was observed in the third reactor configuration studied when 85 mg of 5% $Ni/Al_2O_3$ was packed directly on top of the membrane surface. The $La_{0.2}Ba_{0.8}Fe_{0.8}Co_{0.2}O_{3-\delta}$ perovskite membrane was shown to have a high $O_2$ permeation rate and chemical stability under our experimental reaction conditions.

## Acknowledgments

Financial support for the WPI Center for Inorganic Membrane Studies from Amoco Chemical Company through the Natural Gas University Program is gratefully acknowleged. The authors also thank Dr. Marina R. Pascucci of the Materials Science and Engineering Department, WPI, for many useful discussions about materials synthesis.

## Literature Cited

Alqahtany, H., D. Eng, and M. Stoukides, "Synthesis Gas Production from Methane over an Iron Electrode in a Solid Electrolyte Cell," *J. Electrochem. Soc.*, **140**, 1677 (1993).

Ashcroft, A. T., A. K. Cheetham, J. S. Foord, M. L. H. Green, C. P. Grey, A. J. Murrell, and P. D. F. Vernon, "Selective Oxidation of Methane to Synthesis Gas Using Transition Metal Catalysts," *Nature*, **344**, 319 (1990).

Balachandran, U., J. T. Dusek, R. L. Mieville, R. B. Poeppel, M. S. Kleefisch, S. Pei, T. P. Kobylinski, C. A. Udovich, and A. C. Bose, "Dense Ceramic Membranes for Partial Oxidation of Methane to Syngas," *Appl. Catal. A: Gen.*, **133**(1), 19 (1995).

Blank, D. H. A., H. Kruidhof, and J. Flokstra, "Preparation of $YBa_2Cu_3O_{7-\delta}$ by Citrate Synthesis and Pyrolysis," *J. Phys. D: Appl. Phys.*, **21**, 226 (1988).

Blanks, R. F., T. S. Wittrig, and D. A. Peterson, "Bidirectional Adiabatic Synthesis Gas Generator," *Chem. Eng. Sci.*, **45**, 2407 (1990).

Bouwmeester, H. J. M., H. Kruidhof, A. J. Burggraaf, and P. J. Gellings, "Oxygen Semipermeability of Erbia-stabilized Bismuth Oxide," *Solid State Ionics*, **53-56**, 460 (1992).

Dissanayake, D., M. P. Rosynek, K. C. C. Kharas, J. H. Lunsford, "Partial Oxidation of Methane to Carbon Monoxide and Hydrogen over a $Ni/Al_2O_3$ Catalyst," *J. Catal.*, **132**, 117 (1991).

Dissanayake, D., K. C. C. Kharas, J. H. Lunsford, and M. P. Rosynek, "Catalytic Partial Oxidation of Methane Over Ba-Pb, Ba-Bi, and Ba-Sn Perovskites," *J. Catal.*, **139**, 652 (1993).

Fox, J. M., III, "The Different Catalytic Routes for Methane Valorization: An Assessment of Processes for Liquid Fuels," *Catal. Rev. Sci. Eng.*, **35**, 169 (1993).

Hazbun, E. A., "Ceramic Membrane and Use Thereof for Hydrocarbon Conversion," U.S. Patent No. 4,827,071 (1989).

Hickman, D. A., and L. D. Schmidt, "Production of Syngas by Direct Catalytic Oxidation of Methane," *Science*, **259**, 343 (1993).

Kruidhof, H., H. J. M. Bouwmeester, R. H. E. v. Doorn, and A. J. Burggraaf, "Influence of Order-Disorder Transitions on Oxygen Permeability through Selected Nonstoichiometric Perovskite-Type Oxides," *Solid State Ionics*, **63-65**, 816 (1993).

Mizusaki, J., M. Yoshihiro, S. Yamauchi, and K. Fueki, "Nonstoichiometry and Defect Structure of the Perovskite-type Oxides $La_{1-x}Sr_xFeO_{3-\delta}$," *J. Solid State Chem.*, **58**, 257 (1985).

Nakamura, T., G. Petzow, and L. J. Gauckler, "Stability of the Perovskite Phase $LaBO_3$ (B = V, Cr, Mn, Fe, Co, Ni) in a Reducing Atmosphere, I. Experimental Results," *Mat. Res. Bull.*, **14**, 649 (1979).

Ng, M. F., T. L. Reichert, R. W. Schwartz, and J. P. Collins, "Fabrication of $SrCo_{0.5}FeO_x$ Oxygen Separation Membranes on Porous Supports," Int. Conf. on Inorganic Membranes, Gatlinburg, Tenn. (1996).

Pei, S., M. S. Kleefisch, T. P. Kobylinski, J. Faber, C. A. Udovich, V. Zhang-McCoy, B. Dabrowski, U. Balachandran, R. L. Mieville, and R. B. Poeppel, "Failure Mechanisms of Ceramic Membrane Reactors in Partial Oxidation of Methane to Synthesis Gas," *Catal. Lett.*, **30**, 201 (1995).

Phillies, G. D. J., "Quasielastic Light Scattering," *Anal. Chem.*, **62**(20), 1049A (1990).

Rostrup-Nielsen, J. R., "Syngas for $C_1$-Chemistry, Limits of the Steam Reforming Process," *Studies in Surface Science Catalysis*, Vol. 36, *Methane Conversion*, D. M. Biddy, C. D. Chang, R. F. Howe, and S. Yurchak, eds., Elsevier, Amsterdam, p. 73 (1988).

Supp, E., "Lurgi Concepts for Methanol Plants," *Proc. World Methanol Conf.*, Houston, TX (1989).

Tejuca, L. G., J. L. G. Fierro, and J. M. D. Tascon, "Structure and Reactivity of Perovskite-Type Oxides," *Advances in Catalysis*, Vol. 36, D. D. Eley, H. Pines, and P. B. Weisz, eds., Academic Press, New York, p. 237 (1989).

ten Elshof, J. E., H. J. M. Bouwmeester, and H. Verweij, "Oxidative Coupling of Methane in a Mixed-conducting Perovskite Membrane Reactor," *Appl. Catal. A: Gen.*, **130**, 195 (1995).

Teraoka, Y., H.-M. Zhang, S. Furukawa, and N. Yamazoe, "Oxygen Permeation through Perovskite-type Oxides," *Chem. Lett.*, 1743 (1985).

Teraoka, Y., T. Nobunaga, and N. Yamazoe, "Effect of Cation Substitution on the Oxygen Semipermeability of Perovskite-type Oxides," *Chem. Lett.*, 503 (1988).

Tsai, C. Y., Y. H. Ma, W. R. Moser, and A. G. Dixon, "Modeling and Simulation of a Nonisothermal Catalytic Membrane Reactor," *Chem. Eng. Commun.*, **134**, 107 (1995a).

Tsai, C. Y., Y. H. Ma, W. R. Moser, and A. G. Dixon, "Simulation of Nonisothermal Catalytic Membrane Reactor for Methane Partial Oxidation to Syngas," *Proc. Int. Conf. on Inorganic Membranes*, Y. H. Ma, ed., WPI, Worcester, MA, p. 271 (1995b).

Tsai, C. Y., "Perovskite Dense Membrane Reactors for the Partial Oxidation of Methane to Synthesis Gas," PhD Diss., Worcester Polytechnic Institute, Worcester, MA (1996).

Tsai, C. Y., A. G. Dixon, W. R. Moser, M. R. Pascucci, and Y. H. Ma, "$La_{1-x}A'_xFe_{1-y}Co_yO_{3-\delta}$ (A' = Ba, Sr, Ca) Dense Perovskite Membrane Synthesis, Applications and Characterization," *J. Amer. Ceram. Soc.*, in press (1996).

Vermeiren, W. J. M., E. Blomsma, and P. A. Jacobs, "Catalytic and Thermodynamic Approach of the Oxyreforming Reaction of Methane," *Catal. Today*, **13**, 427 (1992).

Voorhoeve, R. J. H., *Advance Materials in Catalysis*, J. J. Burton and R. L. Garten, eds., Academic Press, New York, p. 129 (1977).

Xia, C., T. L. Ward, R. W. Schwartz, and P. Atanosova, "Dense Mixed-Conducting Stabilized $ZrO_2$ and Perovskite Ceramic Membranes Fabricated by Aerosol-Assisted Chemical Vapor Deposition," Int. Conf. on Inorganic Membranes, Gatlinburg, TN (1996).

Zhang, H. M., Y. Shimizu, Y. Teraoka, N. Miura, and N. Yamazoe, "Oxygen Sorption and Catalytic Properties of $La_{1-x}Sr_xCo_{1-y}Fe_yO_3$ Perovskite-Type Oxides," *J. Catal.*, **121**, 432 (1990).

*Manuscript received Oct. 28, 1996, and revision received Apr. 4, 1997.*